creative commons
COMMONS DEED

저작자표시-비영리-변경금지 2.0 대한민국

이용자는 아래의 조건을 따르는 경우에 한하여 자유롭게

- 이 저작물을 복제, 배포, 전송, 전시, 공연 및 방송할 수 있습니다.

다음과 같은 조건을 따라야 합니다:

저작자표시. 귀하는 원저작자를 표시하여야 합니다.

비영리. 귀하는 이 저작물을 영리 목적으로 이용할 수 없습니다.

변경금지. 귀하는 이 저작물을 개작, 변형 또는 가공할 수 없습니다.

- 귀하는, 이 저작물의 재이용이나 배포의 경우, 이 저작물에 적용된 이용허락조건을 명확하게 나타내어야 합니다.
- 저작권자로부터 별도의 허가를 받으면 이러한 조건들은 적용되지 않습니다.

저작권법에 따른 이용자의 권리는 위의 내용에 의하여 영향을 받지 않습니다.

이것은 이용허락규약(Legal Code)을 이해하기 쉽게 요약한 것입니다.

Disclaimer

dCollection

이학석사 학위논문

Salt concentration effects on stability of residual lithium carbonate on Ni-rich layered oxides

전해질의 농도와 하이니켈 층상계 산화물에서의 잔여 리튬 카보네이트 안정성의 상관관계 분석

2021년 2월

서울대학교 대학원

화학부 분석화학 전공

고 동 혁

이학석사 학위논문

Salt concentration effects on stability of residual lithium carbonate on Ni-rich layered oxides

지도교수 임 종 우

이 논문을 이학석사 학위논문으로 제출함

2021년 2월

서울대학교 대학원

화학부 분석화학 전공

고 동 혁

고동혁의 이학석사 학위논문을 인준함

2021년 2월

위원장 정 택 동 (인)

부위원장 임 종 우 (인)

위원 이 동 환 (인)

Abstract

Salt concentration effects on stability of residual lithium carbonate on Ni-rich layered oxides

DongHyuk Ko

Analytical Chemistry in Department of Chemistry

Graduate School

Seoul National University

The concentration effect of $LiPF_6$, EC (ethylene carbonate) DMC (dimethyl carbonate) electrolyte on the stability of residual lithium carbonate is investigated. Ni-rich layered oxides are widely investigated due to their high energy density among cathode materials. However, they suffer from residual lithium carbonate at the surface which are produced during the synthesis as an unwanted biproduct or during storage in ambient air conditions. This residual lithium carbonate reduces the cyclability and has increased safety issues when decomposed during the cycle. Thus, such adverse effects of residual lithium carbonate are one of the widely investigated issues. While one can assume that transformation of lithium carbonate at the interface between electrolyte and Ni-rich layered oxides can be governed by electrolytes, salt concentration effect has not been clearly investigated. Herein, we study the decomposition of lithium carbonate via an online electrochemical mass spectrometry study (OEMS). The experiments show an increased decomposition at low concentrations of 0.2 M, with a decreased start of

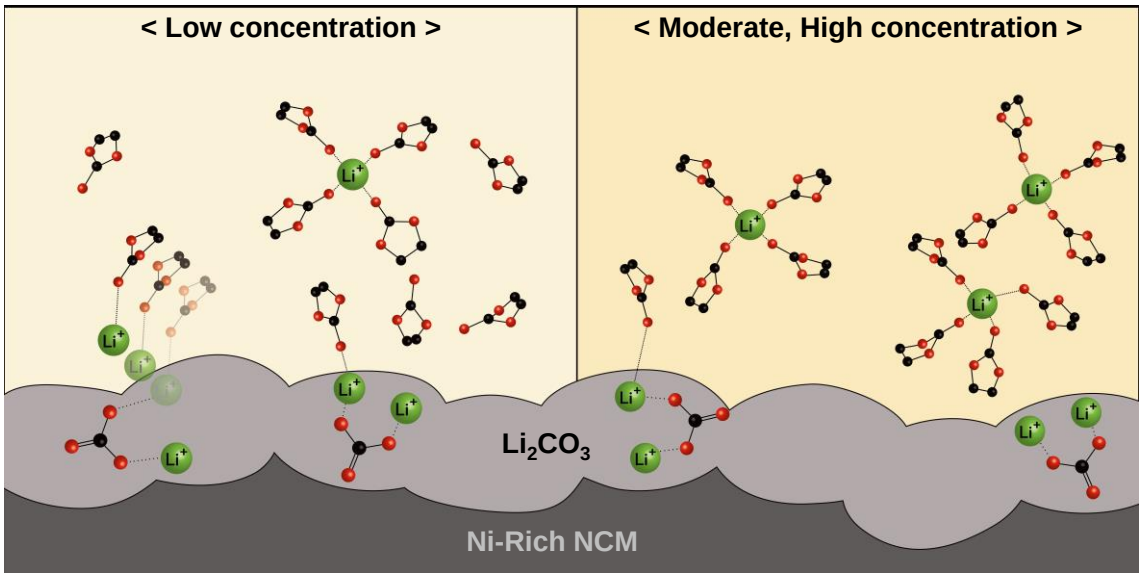

Scheme 1: Electrical decomposition of residual lithium carbonate facilitated by low concentration.

evolution potential compared to moderate and high concentrations of 1 M and 2 M. XPS results further support increased lithium carbonate decomposition at low concentrations. This is hypothesized by the activation energy lowering effects of uncoordinated ethylene carbonate effectively binding to the surface of lithium carbonate residues. The observance of uncoordinated ethylene carbonate predominantly at low concentrations supports our hypothesis. Impacts of increased decomposition reaction is confirmed with electrochemical data and electrochemical impedance spectroscopy.

Keywords: Residual lithium carbonate /Concentration effects /Online electrochemical mass spectrometry /X-ray Photoemission Spectroscopy

Student Number: 2019-29866

Table of Contents

1. Introduction

Increasing energy consumption and its impact on environmental welfare have created high demands for reversible and sustainable energy storage devices. Lithium-ion batteries (LIBs) have been explored to meet these demands in various fields, including portable electric devices, electric vehicles, and stationary energy storage systems,[1,2] owing to properties such as high energy density, safety, high coulombic efficiency, and long lifetime.[2,3]

Among the various LIB cathode materials, Ni-rich layered oxides have been widely investigated because of their high energy density.[3] However, their synthesis with excess lithium precursors results in increased residual lithium carbonate impurities on the surface.[4,5] The tendency of trivalent Ni^{3+} to reduce into divalent Ni^{2+} produces more lithium residues on the surface if stored in ambient air,[6,7,8] which subsequently leaves residual lithium carbonates (Li_2CO_3) primarily on the surface.[7,8] The presence of residual Li_2CO_3 is inconvenient because the electrochemical oxidation of residual lithium during the cycle could produce CO_2, and increase the cell pressure and aggravate battery safety.[9] Furthermore, the side products stemming from the decomposition can destabilize the cathode–electrolyte interface[10] and result in cycle degradation.[11,12] Many studies have reported that the removal of residual lithium before the assembly of electrodes and batteries is crucial to extend cyclability. However, challenges remain in achieving complete lithium residue removal.[3,6] Therefore, inhibiting the decomposition of lithium carbonate during cycling is important. A detailed investigation of electrolytes, which play a crucial role in the stability and transformation dynamics of the surface lithium carbonate,[13] has not been conducted. Chemical properties, such as electrolyte

coordination environments, are known to be affected by salt concentration, which has led to studies on the manipulation of salt concentration to substantially regulate the electrode–electrolyte interphase at the lithium metal electrode.[14,15] However, studies on the effects of salt concentration on the interface or interphase stability at the cathodes are lacking.

In this study, the effects of salt concentration on the stability of residual Li_2CO_3 on the surface of Ni-rich layered oxides are reported. Real-time gas evolution measurements via online electrochemical mass spectrometry (OEMS) during the initial cycles and surface chemical composition analysis via X-ray photoemission spectroscopy (XPS) after the initial cycles revealed the enhanced decomposition of residual lithium at low concentrations. This decomposition can be attributed to the adhesion of free ethylene carbonate (EC) to the surface of the cathodes, which lowers the activation energy, whereas the more stable adhesion of lithium-solvating ethylene carbonate to the surface protects the decomposition in higher-concentration electrolytes. Raman spectroscopy shows that EC is largely uncoordinated at low concentrations, supporting our hypothesis. Electrochemical cyclability and EIS spectroscopy data further reveal the detrimental effect of such decompositions enhanced by low salt concentrations.

2. Result and Discussion.

OEMS data

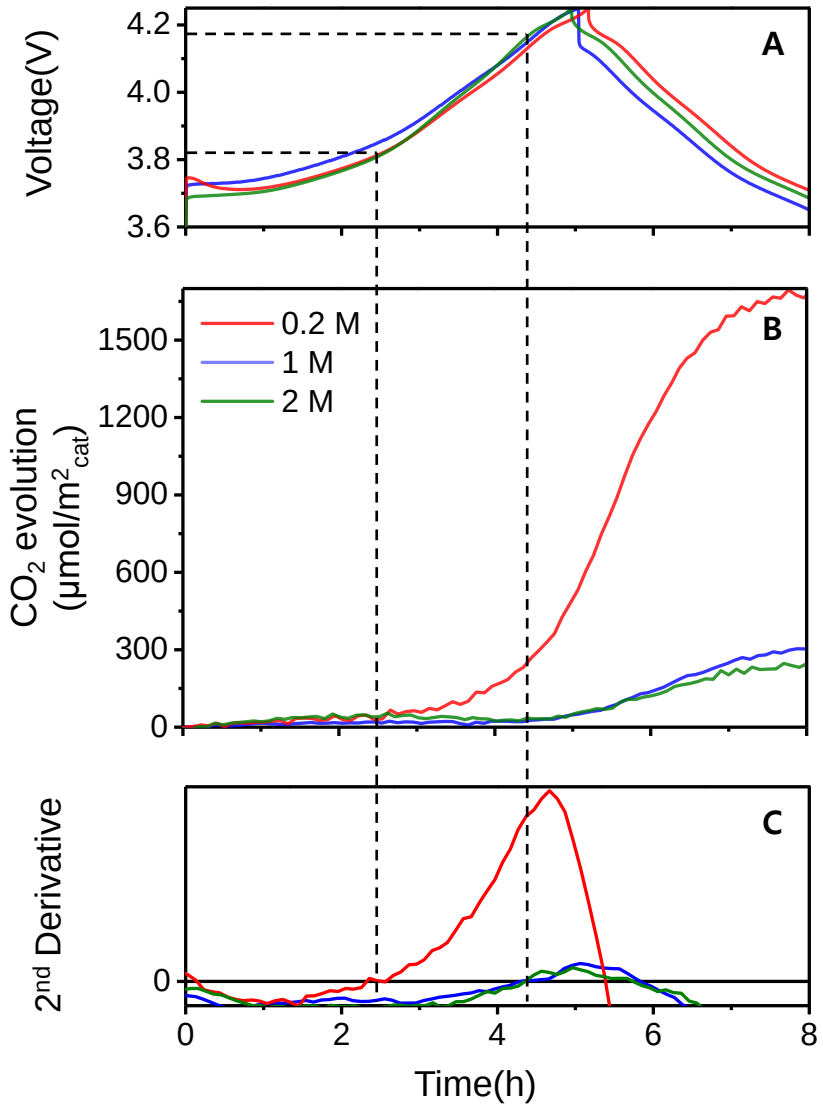

Figure. 1: (A) Voltage profile of different electrolytes (B) in-situ CO_2 evolution representing lithium carbonate decomposition and (C) second derivative of CO_2 to verify start of evolution potential.

To observe the effects of concentration on gas evolution, an OEMS setup was developed to perform in situ quantification of residual Li_2CO_3 decomposition. In our OEMS, the standard leak interfaces allows a small fraction of gas sampled from the

headspace of the cell, similar to a previous setup.[16] The mass spectrometry signal was correlated with the partial pressure of the standard gases at varying concentrations. The total gas pressure was also varied, which affected the correlation and completed the three-dimensional calibration surface contour. Li_2CO_3 decomposes directly to gaseous CO_2 during the first cycle between 3.0–4.3 V vs Li/Li^+ and is the major source of CO_2 within this voltage range.[17] Details on the quantification process could be found in Supplementary data 4. Commercial $LiNi_{0.8}Co_{0.1}Mn_{0.1}O_2$ (NCM811) powders purchased from Toshima.Inc (Experimental) were mixed with conductive carbon additives and polyvinylidene fluoride (PVDF) binder in a weight ratio of 8:1:1; lithium metal anodes were used in this study. The $LiPF_6$ concentration is varied (0.2 M, 1 M, and 2 M) in a 1:1 volume ratio of ethylene carbonate (EC) and dimethyl carbonate (DMC). Figure. 1(A) shows the voltage profiles of the NCM811 half-cells during the operation, and Figure. 1 (B) shows the corresponding CO_2 evolution curves. The 1 M and 2 M half-cells are seen to evolve similar volumes of CO_2, with a total of 300 μmol/m^2_{cat} and 250 μmol/m^2_{cat}, respectively. However, CO_2 evolution in the 0.2 M half-cell is ~1700 μmol/m^2_{cat}. Also, the start of evolution potential is different with electrolytes. The start of evolution of CO_2 may be defined where the second derivative of measured gas is equal to zero (Figure. 1(C)),[18] with matching potentials found (Figure. 1(A)). The sudden rise of gas evolution can be detected when the first and second derivative reaches local minimum and zero, respectively.[18] 0.2 M started to evolve at 2.5 hours corresponding to a potential of 3.82 V vs Li/Li^+, compared to 4.4 hour corresponding to 4.18 V and 4.2 V vs Li/Li^+ at 1 M and 2 M electrolytes. Although the start of evolution potential of Li_2CO_3 decomposition observed at 4.2 V vs. Li/Li^+ agrees with previous reports,[19,20,21] cathodic decomposition near the reduction potential of 3.82 V has yet not been reported on NCM surfaces. The

suggested reaction is as follows:

$2\ Li_2CO_3 \rightarrow 4\ Li^+ + 4\ e^- + 2\ CO_2 + O_2$ ..... $E^0 = 3.82$ V vs Li/Li^+ Eq.1

The potential dependence in our experiments strongly support this electrochemical decomposition reaction. Other reports show that only CO_2 and not CO is evolved while electrochemical decomposition.[10,17] Therefore, mechanisms that involve CO products are not likely. Since the major source of carbon dioxide derives from residual Li_2CO_3 and 1 mole decomposition of Li_2CO_3 produces 1 mole of CO_2,[10,17] the quantities of gaseous CO_2 observed in our experiments directly correlate to decomposition of residual Li_2CO_3.

Other studies show that impurities existing could be a major source of Li_2CO_3 decomposition.[4,11] The proposed chemical decomposition with HF and protons is the following Eq. 2, and Eq. 3,

$Li_2CO_3 + 2\ H^+ \rightarrow 2\ Li^+ + H_2O + CO_2$ ..... Eq. 2

$Li_2CO_3 + 2\ HF \rightarrow 2\ LiF + H_2O + CO_2$ ..... Eq. 3

The produced water reacts with the salt, $LiPF_6$, to reproduce HF with the following equations Eq. 4and Eq. 5,

$LiPF_6 + H_2O \rightarrow LiF + 2\ HF + POF_3$ Eq.4

$LiPF_6 + H^+ \rightarrow Li^+ + HF + PF_5$ Eq.5

However, this chemical decomposition is not the main source of decomposition in our experiment. Since the electrolytes of the experiment were produced from the same materials with the same ratio of solvents, it is expected that the extent of impurities is relevantly similar for solvents. Therefore, if the impurities were the source of decomposition, there would be no correlation observed with concentration. Also, the

electrolyte materials were kept in the glovebox and never exposed to ambient air or moisture to expect such impurities. Considering the experimental conditions, therefore, Li_2CO_3 decomposition deriving from impurities would not be the major cause of the difference in carbon dioxide formation. Similarly, activation of the decomposition of Li_2CO_3 by electrochemical oxidation of electrolyte and electrolyte impurities reported in other papers cannot explain the different start of evolution potentials that were within this experiment.[4] Therefore, rather than a decomposition from impurities, electrochemical decomposition is likely.

X-ray Photoemission Spectroscopy data

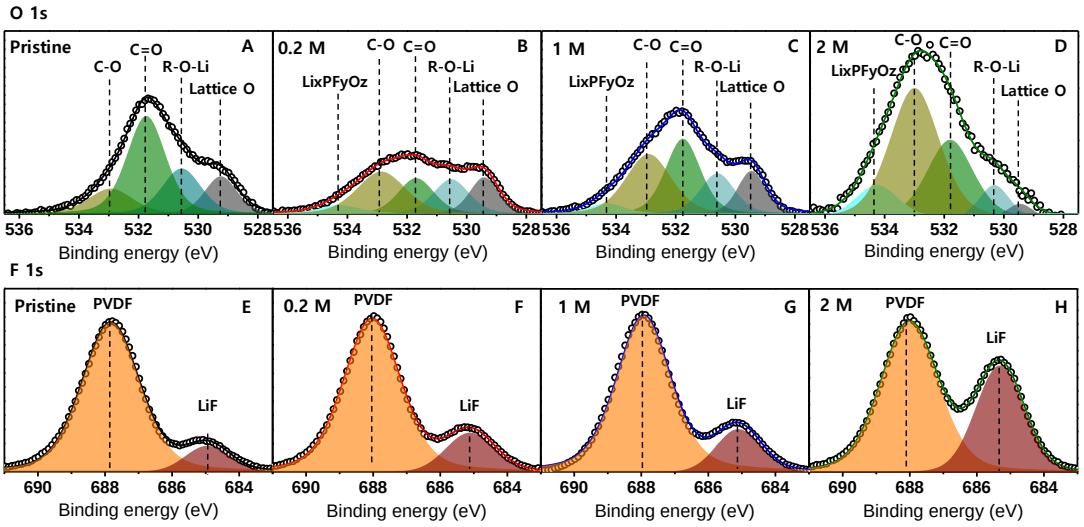

Figure. 2: XPS O 1s spectra of (A) pristine, after 3 cycles of 0.2 C 3.0 V - 4.3 V samples of (B) 0.2 M (C) 1 M, (D) 2 M. F 1S spectra of (E) pristine and after 3 cycles of 0.2 C 3.0 V - 4.3 V samples of (F) 0.2 M (G) 1 M and (H) 2 M

The XPS spectra of the cathode after the initial cycles also reveal increased decomposition of residual Li_2CO_3 at low salt concentrations. The O 1s spectra are shown in Figure. 2 (A–D). Because only Li_2CO_3 has C=O bonds among the cathode materials, the C=O peak intensities at 531.7 eV can be correlated to the relative amount of Li_2CO_3 at the surface and normalized by lattice oxygen for pristine, 0.2 M, and 1 M electrolytes. This can be justified because the lattice oxygen evolution reaction occurs only above 4.5 V vs. Li/Li^+,[22] which implies that no lattice oxygen should be altered or evolved herein. The surface coverage of Li_2CO_3 reduces heavily for the 0.2 M electrolyte, supporting the OEMS results. Each LixPFyOz peak in Figure. 2 (B–D) corresponds to an additional cathode–electrolyte interface (CEI) arising from the salt decomposition reaction, and the C–O peak corresponds to polymeric CEI.[19,21,23] Interestingly, these peaks are largely pronounced for the 2 M electrolyte, suggesting that the CEI increasingly forms on the cathode surface.[24–26] However, this can hamper the assessment of the Li_2CO_3 residue or its solid-state

decomposition product. The accelerated CEI formation in the 2 M electrolyte is further supported by the XPS F 1s peaks shown in Figure. 2 (E–H). LiF, which forms a CEI, is known to be a major decomposition product of $LiPF_6$.[27] The PVDF peaks at 688 eV were used to normalize the LiF peaks at 685 eV. The LiF peak intensities in pristine, 0.2 M, and 1 M samples are similar (Fig. 2 (E–G)). The stark increase in LiF intensities in the 2 M sample (Figure. 2 (H)) indicates enhanced CEI formation.[28] The OEMS and XPS data are in good agreement regarding the decomposition of Li_2CO_3 being facilitated more with 0.2 M than 1 M, whereas the complicated contest between CEI formation and Li_2CO_3 dissociation occurs with the 2 M electrolyte.

Characterization of electrolytes

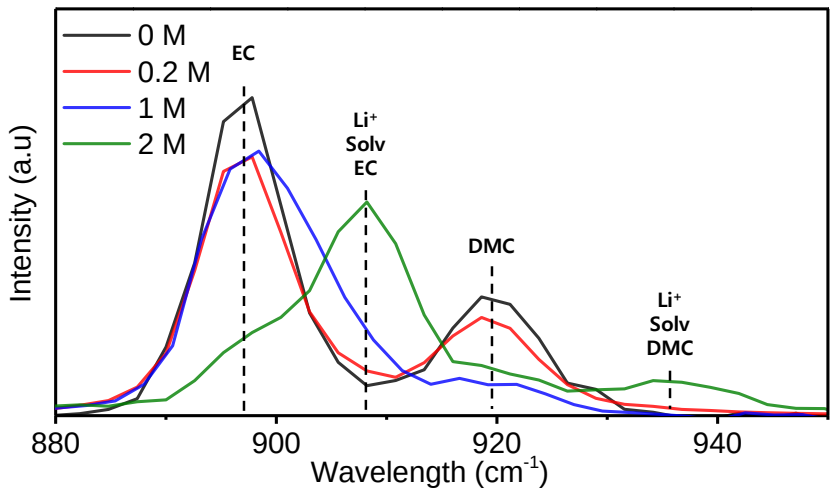

Figure. 3: Raman spectra from 860 cm^{-1} to 950 cm^{-1} of various electrolytes before cycling. Raman peaks of the C-O stretching of free EC (898 cm^{-1}), Li^+ solvated EC (908 cm^{-1}), free DMC (918 cm^{-1}) and Li solvated DMC (937 cm^{-1}) are shown.

Li-ion dissociation from carbonate anions is known to be the rate-limiting step in the oxidative decomposition of Li_2CO_3[10,16] during electrochemical charging. This is because the ionic bonding between Li and carbonate ions is difficult to dissociate. This dissociation can be accelerated if free EC molecules in the electrolyte with high polarity and basicity effectively bind to the Li ion on the surface of Li_2CO_3; this is suspected to lower the kinetic barriers to complete dissociation.[20] The presence of free EC (i.e., EC that does not solvate Li ions in the electrolyte) is dominant at low salt concentrations, which can be confirmed by Raman spectroscopy, a tool of choice for probing the local coordination of electrolyte and Li ions.[29] When EC is coordinated with Li ions in the electrolyte, the C–O stretching mode shifts to a higher energy. The free EC in the 0.2 M cell is largely populated according to the 918 cm^{-1} peaks, in contrast to that in the 1 M and 2 M cells (Figure. 3).

Other properties such as viscosities of the electrolyte are also considered for possible sources of the difference of decomposition. The increase of concentration would affect the viscosity of the electrolyte. Previous papers have predicted that in 1:1 EC:DMC $LiPF_6$ electrolytes, the viscosity of 0.2 M, 1 M, 2 M electrolytes are ~1, 4 and 10 η/mPa·s respectively.[30,31] The significant increase of viscosity reported in higher concentrations would decrease the transport of decomposition products of Li_2CO_3. The slow transport properties and increased concentration gradients could in turn increase the overpotential suggested in some papers.[20] However, the start of evolution potential difference would not be explained by this behavior since there are no decomposition products at the start of decomposition. Therefore, the overpotential caused by the viscosity could not explain our difference in start of evolution potentials fully, and not explain the different stabilities.

Impacts to the long-time performance of LIBs

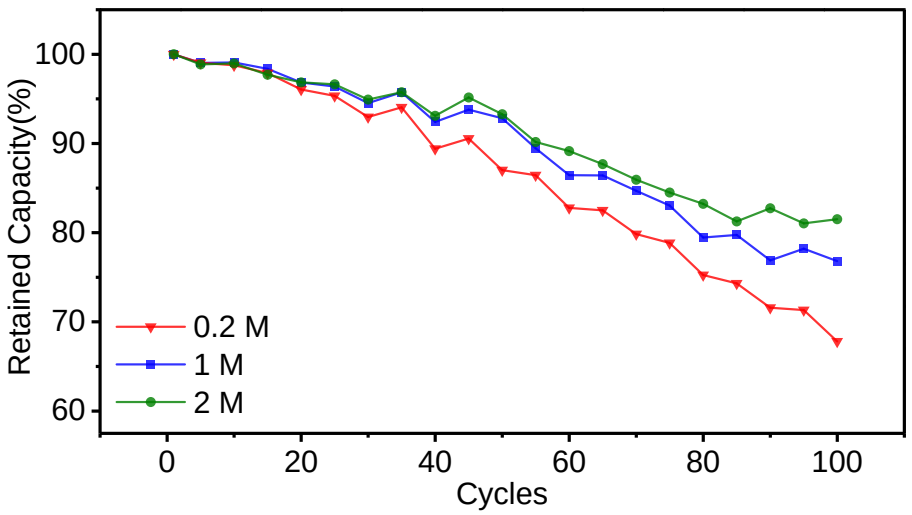

Figure. 4: Retained capacity of NCM811 half cells using various electrolytes.

The impacts of the increased decomposition reactions on cyclability were

investigated, as shown in Fig. 3 (B), to confirm the adverse effects of Li_2CO_3 decomposition with varying salt concentrations.[10–12] All cells had comparable starting discharge capacity slightly over 200 $mAhg^{-1}$, shown in Supporting information 3. However, the 0.2 M cells exhibited the highest capacity retention decay of all the cells (68 %, 78 %, and 83 % after the 100^{th} cycle for 0.2, 1, and 2 M cells, respectively. The rapid capacity fading of 0.2 M cells is attributed to the rapid decomposition of Li_2CO_3 at the interface. The decomposition of Li_2CO_3 involves many side reactions that are detrimental to the cycle life.[14,15] In particular, singlet oxygen was reported as an electrochemical decomposition product of Li_2CO_3[32], which is oxidative and can react with EC to form HF.[30] The production of such side products affects the cycle life and increases impedance.[14,15] Additionally, the 2 M cell is observed to induce a superior cycle life, which is consistent with the XPS results herein; the more thick CEI formed during the initial cycles can stabilize the interface.[24–26]

Electrochemical Impedance Spectroscopy

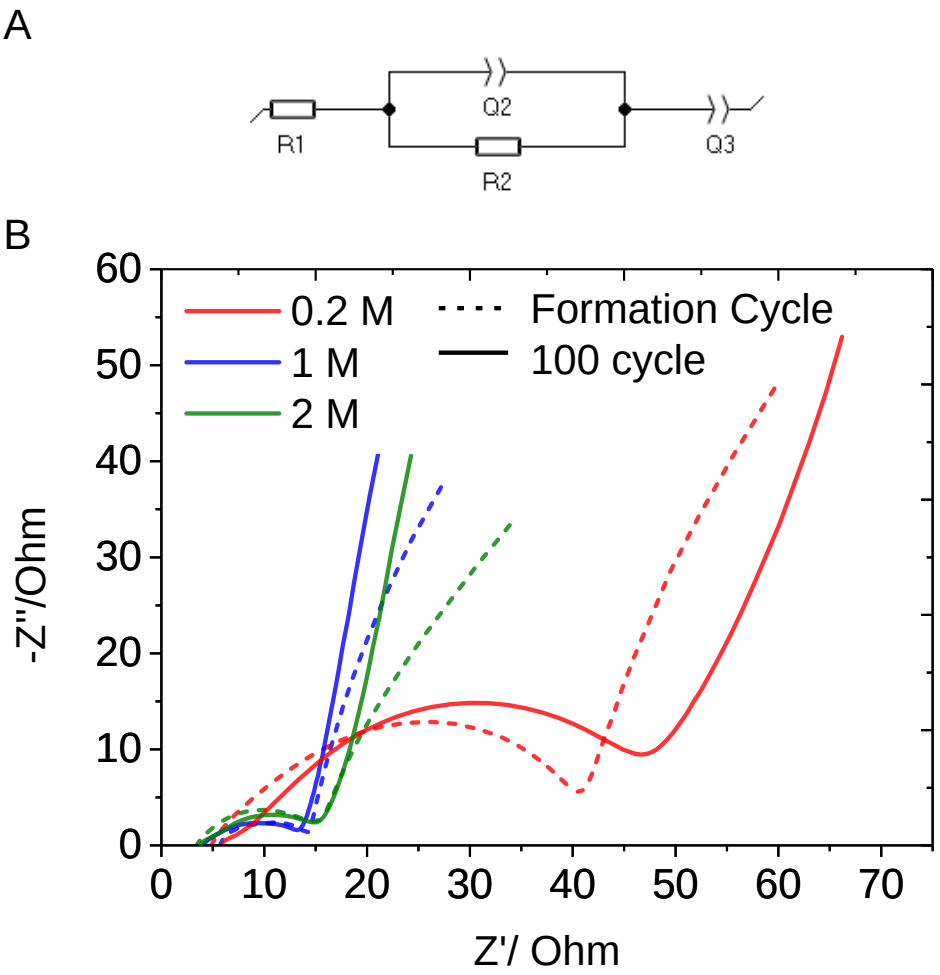

Figure. 5: Corresponding circuit of the cathode interface (A), and its Nyquist EIS spectra (B) after formation cycle (dashed lines) and 100th cycles (solid lines) of various electrolytes

The interfacial impedance at the cathodes was subsequently measured with cycles at varying salt concentrations to assess the effects of residual Li_2CO_3 decomposition on the cycle life. The impedance of each cell was measured from the formation to the 100th cycle shown in Figure. 5(B).[27,33] The equivalent circuit represented in Figure. 5(A) is comprised of one resistor in series to a resistor and a constant phase element (CPE), with an additional CPE at the end. R1 is the solution resistance, and R2 is the combination of contact resistance and the charge transfer resistance of the CEI.[33] Many reports have an additional pair of a resistor and a

CPE to differentiate contact resistance and charge transfer resistance, but the circuit is simplified in this experiment to give a better understanding of the interfacial impedance without artificially fitting values of the circuit.[33,34]

R2 can reflect the aggravated lithium transport through the interfacial layers with cycles. The largest R2 value seen after formation is 0.2 M shown in Figure. 5 (B). This could be from decreased lithium carbonate residues, which have better ion conductivities compared to the electrolyte.[35] This decrease of residual Li_2CO_3 would therefore have increasing resistance on the interfacial layer. However, This value cannot be compared directly between the formation cycles or the 100th cycles because of different ionic conductivities.[34] Therefore, rather than comparing directly between each electrolyte, the increases of R2 from the formation cycle to the 100th cycles are measured. They increase by 89.8 % for 0.2 M while 1 M and 2 M only changed 16.6 % and 20.1 % in Supporting information 5. This increase is consistent with the adverse product effects of decomposition of residual Li_2CO_3. These products remain within the electrolyte and persistently degrade the integrity of interface, leading to increased R2 values.[36]

This result also does not contradict observations seen in OEMS, XPS or Raman data. Li_2CO_3 decomposition would result in less Li_2CO_3 on the surface which has great ion conductivity.[35] Decomposition of Li_2CO_3 could therefore increase R2 values, supporting our data. Meanwhile, reports show the decomposition of Li_2CO_3 leads to increased charge transfer resistance at long-cycled batteries.[4,14,15] This increase of impedance at long cycles is from side products such as HF[14,15,37] that would leach out transition metals and would cause increased charge-transfer resistance. Therefore, the increased impedance spectra shown at long cycles also support more degradation at low concentrations.

Although none of our experiments could show direct evidence of the stability of residual Li_2CO_3 decomposition on Ni-rich layered oxides on their own, the comprehensive understanding of each experiment leads to the conclusion that residual Li_2CO_3 has increased decompositions when concentration is low. OEMS data show an increased CO_2 evolution in low concentrations, with a lower start of evolution potential. The only source of CO_2 within our experiment potential window is from residual Li_2CO_3 decomposition[10,17], therefore, this data gives strong evidence that lower concentrations have reduced the stability of residual Li_2CO_3. This is further observed with XPS results of the cathodes after formation. Residual Li_2CO_3 could be qualitatively assigned with the C=O peak intensities. This shows that in 0.2 M surfaces after initial cycling, there were reduced Li_2CO_3 coverage comparing to pristine surfaces. Meanwhile, the adverse effects on the degradation of Li_2CO_3 to the performance of LIBS are shown in many reports.[14,15] The stark increase of charge transfer resistance and lower retained capacity of our experiments both match with existing reports of decomposition of Li_2CO_3.[14,15] The side products shown with OEMS, the disappearance of existing Li_2CO_3 from XPS and comparison of cyclability and EIS data with existing reports all support that there is increased decomposition at low concentrations. This is caused by the increased surface adhesion of free-EC on residual Li_2CO_3. It is hypothesized that free-EC has lowering effects on the kinetic barrier and therefore increases the rate of the decomposition of residual Li_2CO_3.

3.Conclusion

A comprehensive study of concentration on residual Li_2CO_3 was performed. OEMS and XPS data reveal the acceleration of Li_2CO_3 decomposition at low salt concentrations. This could be attributed to the decrease in the activation energy of the dissociation of Li_2CO_3 by the adhesion of free EC to the cell surface; free EC was not available at moderate and high concentrations. An increase in the decomposition resulted in adverse effects on the cyclability of LIBs and increased the impedance. The results of concentration dependence on the extent of Li_2CO_3 stability could provide insights into the design of future electrolytes and the creation of stable CEIs with better performance.

4.Experimental

Materials & sample preparation

$LiNi_{0.8}Co_{0.1}Mn_{0.1}O_2$ (NCM811) powder was purchased from Toshima Manufacturing.Co. Lithium metal anodes are 0.3 mm thick. The coin cell parts were purchased from Welcos. Inc. Anhydrous dimethyl carbonate (≥99 %) ethylene carbonate (≥99 %) were purchased from Sigma-Aldrich, and anhydrous $LiPF_6$(≤5 ppm) was purchased from Puriel. Whatman GF/F glass fiber was used for separators. All electrolytes are of ethylene carbonate: dimethyl carbonate 1:1 volumetric ratio and were kept in a glovebox to prevent impurities. Electrolytes were kept without light exposure, as it is reported to decompose the electrolyte.[38]

All cells were assembled inside an argon-filled glovebox([O_2] <1 ppm, [H_2O] <0.1 ppm. The cathode slurry was made with active material: conducting carbon: PVDF weight ratio of 8:1:1 and was doctor bladed 20 μm thick and left to dry for 12 hours under dry air conditions of 120 ℃, increasing the surface Li_2CO_3 level. After slurries were prepared, they were stored in the glovebox to prevent further formation of Li_2CO_3. Coin cells were assembled with diameters of 12 mm cathode, 17 mm separator and 14 mm diameter lithium anodes, and OEMS cells were assembled with 38 mm cathode with 16 2 mm diameter holes (for improved gas flow, see supplementary data), 47 mm separator and 40 mm lithium anode. 200 μl of electrolyte was used for coin cells and 1 ml for OEMS cells.

OEMS

The HPR-40 OEMS device was purchased from Hiden Analytical, and was modified to fit battery gas analysis, which the specifications are in the Supplementary data 1,2. Differences in temperature and pressure within the cell were calibrated using a 3D contour plot using standard gases of 500, 1000, and 2000 ppm of various gases of different inlet pressures which was verified to be accurate within our experimental range shown in Supporting information 4. Electrochemical data was collected with VSP-200, and the m/z signals were collected with the Hiden analytical software.

All experiments with the OEMS had a OCV step for 5 hours before the experiment to stabilize the signals from the OEMS equipment.

XPS

Coincells of 0.2 M, 1 M and 2 M were cycled at 40 mA/g current for three cycles between 4.3 V and 3.0 V, with a hold step at the peak voltages. Then the cells and a fresh cathode sample were disassembled and rinsed with DMC and sealed in an argon environment. All XPS tests are conducted by Korea Institute of Ceramic Engineering and Technology with an argon environment to ensure the cathode electrolyte interface (CEI) does not change. After subtraction of a Shirley background, the peaks are fit using a nonlinear, least-squares routine with mixed Gauss–Lorentz function of 70% Gaussian and 30 % Lorentzian. An asymmetric line shape is introduced to precisely fit the peak in both O 1s and F 1s regions.

Raman Spectroscopy

Raman spectroscopy was carried out with a Raman microscopy system (HEDA, NOST, Ar laser at 532 nm). The laser was focused on the samples using a confocal microscope equipped with a 50x objective lens (MPLFLN). The laser was calibrated

using a silicon standard with its peak at 520.7 cm^{-1}.

Electrochemical data / EIS spectroscopy

All coin cells were cycled with Wonatech WBCS3000L. For the cyclability test, the coin cells were charged with a current of 40 mA/g to 4.3 V and was held at 4.3 V until the current dropped to 10 mA/g. Then they were discharged to 3.0 V with the same current and was held until the current dropped to 10 mA/g. Three consecutive formation cycles were done with this manner. and the current was increased to 200 mA/g for both charging and discharging for 100^{th} cycles. EIS spectroscopy from 1 MHz to 1.2 Hz was measured with Biologic VSP300 potentiostat right after the discharge step of the formation cycle, and at the discharge state after 100^{th} cycles with the same coin cell.

5.Supplementary data

1.OEMS cell design

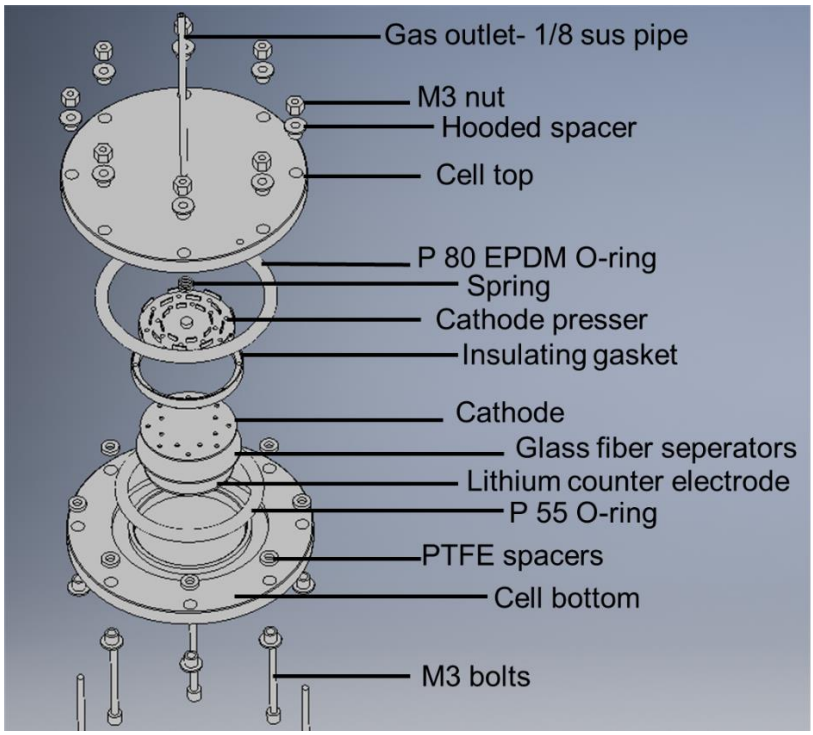

Supplementary Figure. 1 : Cell design

Supplementary Figure. 1 shows the setup of our OEMS cell. There is a 1/8-inch SUS pipe connected to the OEMS setup at the center of the cell top, which is also made of SUS metal. The cell top also has an indentation to fit the p80 backup o-ring, to ensure there are no gas leaks. The spring is for applying pressure while operating the cell, as well as acting as an electric contact to operate electrochemistry. The pressure is in accordance with commercial coin cell pressure, quantified by careful calculations. The cathode presser is 40 mm in diameter, slightly larger than the cathode and is made of SUS metal. If there are no holes in the cathode, side reactions and gas species that evolved at the center of the cathode would have to be carried to the perimeter of the cathode presser, increasing latency and potential side reactions involving gas species. To reduce this

problem, there are 16 2 mm diameter holes that are in the presser and cathode which are aligned. The cathode slurry is cut with a lab-made Thompson knife. Glass fiber separators, the insulating gasket and PTFE spacers electrically insulate the top part of the cell from the bottom of the cell. A 40 mm diameter lithium counter electrode is placed at the center of the cell bottom, which is also SUS, and has an indentation for the P55 main O-ring. The O-rings are made of EPDM, which is electrochemically stable in the experimental conditions, although they do not contact directly with any electrolyte. The whole system is screwed tight with 8 M3 bolts and nuts which are made of SUS to ensure the cell is gastight. The bolts are electrically protected with PTFE hooded spacers and the PTFE spacers, and are not in direct contact with either the top or the bottom cell to ensure electrochemistry. The total cell volume is designed to be minimum to increase the signal intensity of gaseous side products, and the head space volume including the sus 1/8 tubing is ~5.3 cm^{-3} which were calculated using the CAD design and length of tubing.

2. OEMS interface design

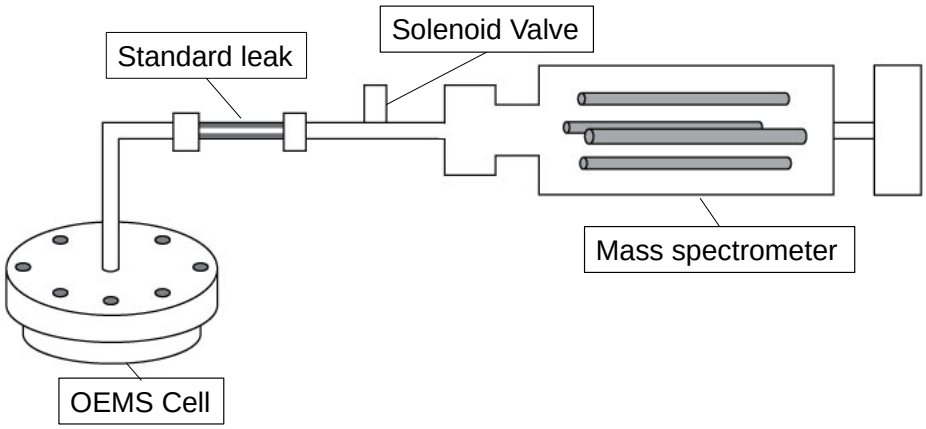

Supplementary Figure. 2: Online mass spectrometer setup

The OEMS cell is attached to a standard leak that has a flow rate of 1 ul/s, assuming that the pressure of the cell is 1 atm and 25 ℃, and only consists of Argon. A

solenoid valve is attached to protect the mass spectrometer from sudden increases of pressure, and the mass spectrometer pressure is maintained below $10E^{-7}$ Torr. Since the standard leak's flow rate depend on the inlet pressure, continuous extraction would lower the inlet pressure and decrease flow rate. To quantify this decreased flow rate with the actual quantity of gaseous products, a contour of the dependance of mass spectrometer signals with both the quantity of real gas and flow rate must be considered. The contour plot used to quantify experimental data are shown in Supplementary data 4.

3.Formation cycle comparison of coin cells and OEMS cells

	0.2 M	1 M	2 M
Specific charge capacity (mAh g^{-1})	226.88	226.84	225.48
Specific discharge capacity (mAh g^{-1})	201.63	203.79	202.43
Coulombic efficiency (%)	88.87	89.84	88.13

Supplementary Table 1: Coin-cell formation cycle specific charge capacity, specific discharge capacity and coulombic efficiencies of various electrolytes.

The formation cycle data of coin cells are presented in Supplementary Table 1. This agrees with existing reports of NCM 811 cathode materials[11]. However, the fast decrease of retained capacity experienced with all our experiments shown in Figure. 4 is deriving from adverse effects of increased Li_2CO_3 formation during processing[11].

	0.2 M	1 M	2 M
Specific charge capacity (mAh g^{-1})	216.85	225.66	222.33
Specific discharge capacity (mAh g^{-1})	184.60	196.01	189.61
Coulombic efficiency (%)	85.12	86.86	85.29

Supplementary Table 2: OEMS formation cycle specific charge capacity, specific discharge capacity and coulombic efficiencies of various electrolytes.

OEMS formation cycle data are presented in Supplementary Table 2. Comparing the coulombic efficiency with Supplementary Table 1, the coulombic efficiencies of the OEMS cell are ~3 % lower than coin cell data. A uniform decrease in both the specific charge capacity and discharge capacity would be correlated to different dimensions and slight differences in C-rate, caused by weight measuring errors. Since the dimensions of the DEMS cell do not exactly match coin cells, there would be different amounts of

lithium anode surface, and cathode surfaces. This in turn would cause the difference in coulombic efficiency. However, the cell voltage profile of NCM811 shown in Figure. 1A shows characteristic profiles of NCM811, and therefore the electrochemistry does not seem to differ much. The difference in specific charge capacity and discharge capacity is from measurements of the slurry's active weight.

4.OEMS quantification

Assuming a homogeneous sampling of gas species through the standard leak,[39] the ppm value of the gas products within the headspace will remain equal. However, the standard leak would have varying flowrates since a continuous flow of samples are introduced to the mass spectrometer. To quantify the concentration of CO_2, the mass spectrometer signals of various pressures of standard gas with 500,1000, and 2000 ppm of CO_2 and the rest consisting of Argon is experimented. The surface of this 3D plot is shown in Supplementary Figure. 3, where t is the cell pressure, ppm is the standard gas concentrations and Torr is the actual signals of the mass spectrometer by secondary electron multipliers.

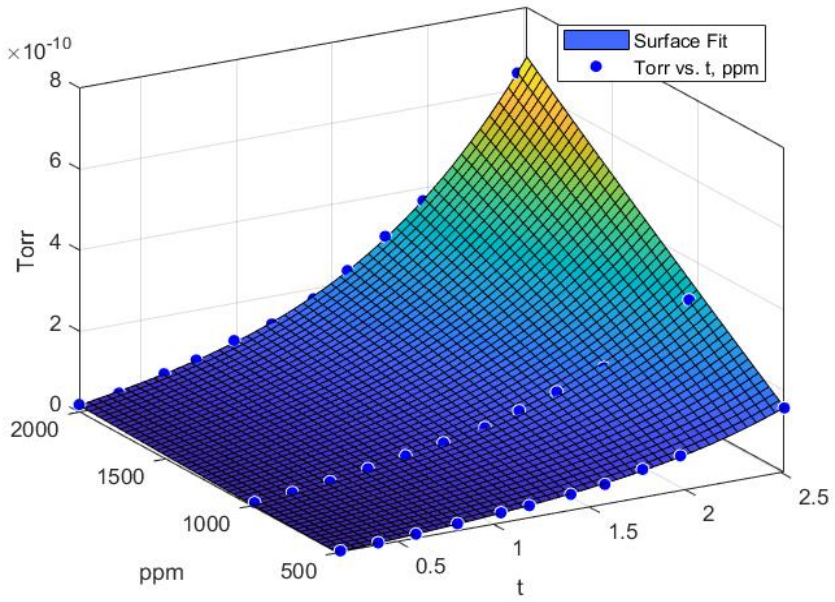

Supplementary Figure. 3: Inlet pressure (t) vs ppm vs mass spectrometer signal (Torr)

Using this 3D plot, the signals of the mass spectrometer with the inlet pressure is in turn calculated into actual ppm values of the cell. The dynamic range and reliable quantification region from the standardization 3D plot are after 5 hours of stabilization and within 25 hours of experiment, since the fitted 3D curve has huge variance in low cell pressures. The cell after 25 hours of sampling was 0.8 atm, meaning that the decrease in flow rate affect the signal intensity of the mass spectrometry. To test our 3D plot, a blank cell with 1 ml of 1M electrolyte is quantified, shown in Supplementary Figure. 4.

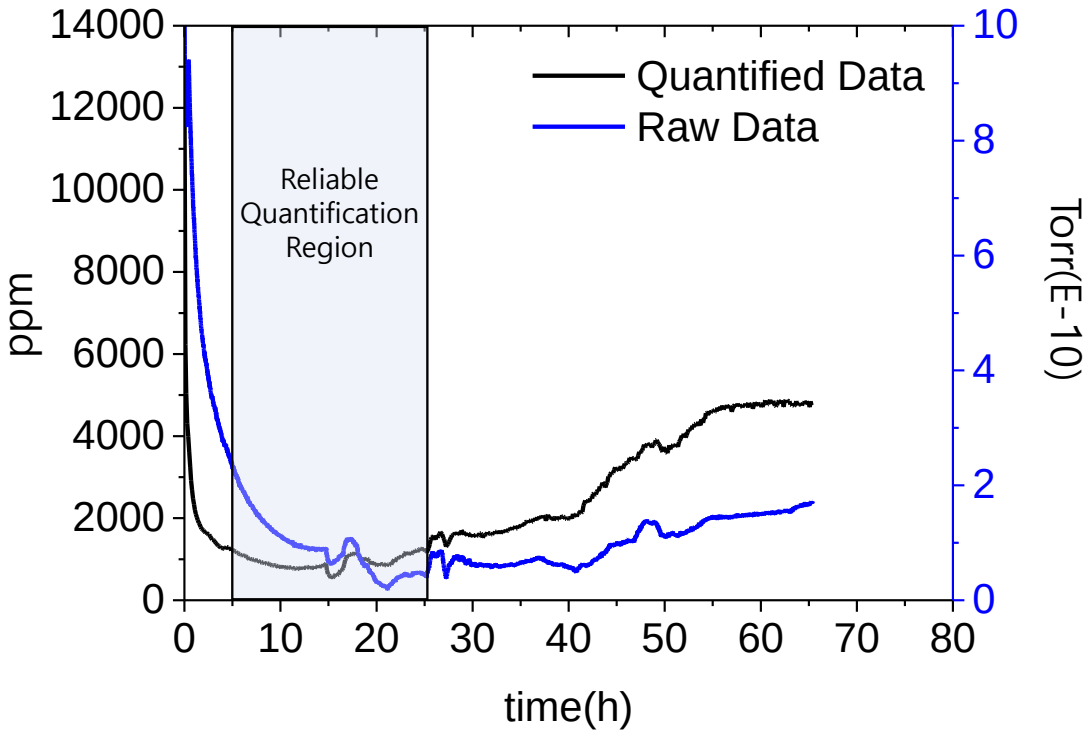

Supplementary Figure. 4: Raw data and quantified data of CO_2 signals of 1 ml 1 M in OEMS cell

The continuous value of 700 ppm within the reliable quantification region is from the partial pressure of solvent species such as dimethyl carbonate which have fragmentations of CO_2. A constant value of this quantified data in this extremely low vacuum shows that the quantification of our system is reliable. However, there are aberrations within the experiment that were detected in many of our quantification experiments and actual experiments. The sudden change seems to be random in time but are easily ruled out by equal changes detected in the vacuum level since the vacuum could vary in time. These sudden changes were ruled out by repetitive experiments with identical conditions.

5.EIS fitting values.

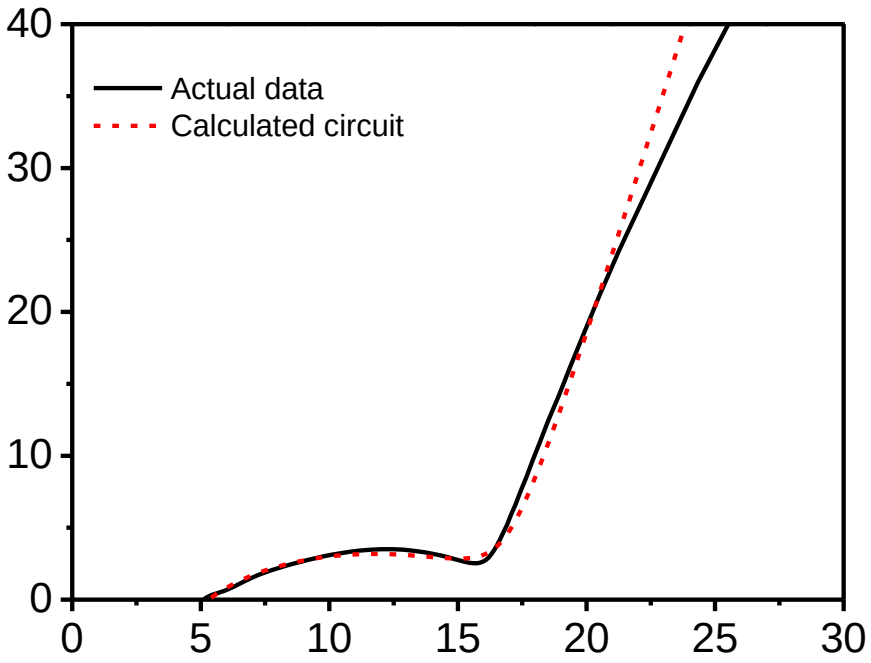

Supplementary Figure. 5: Circuit fitting values of 1 M 100th cycle data

The Nyquist plot of the actual data and calculated circuit are shown in Supplementary Figure. 5. It shows that the observed impedance correlates well with our calculated circuit. The values of the circuit components are in Supplementary Table 3.

	After 3 initial cycles			100th cycle		
	0.2 M	1 M	2 M	0.2 M	1 M	2 M
R1	4.66	5.57	3.46	7.89	5.31	3.84
Q2	6.3.E-05	1.8.E-04	1.4.E-04	3.0.E-04	5.1.E-04	8.0.E-04
a2	0.72	0.65	0.69	0.60	0.60	0.52
R2	24.66	8.91	11.12	46.21	10.39	13.36
Q3	7.4.E-03	5.0.E-03	6.5.E-03	3.8.E-03	3.7.E-03	4.8.E-03
a3	0.56	0.81	0.70	0.84	0.87	0.89

Supplementary Table 3: Circuit component values fitted to measured data.

R2 values are responsible for the ion transfer behavior at the active material and CEI interface. While there is an increase of R2 in 0.2 M from 24.66 Ohm to 46.21 Ohm, other electrolytes do not have such increases. The difference in R2 is 89.8 %,16.6 % and 20.1 % for 0.2 M, 1 M, and 2 M electrolytes. Direct comparison of charge transfer resistances cannot be done between the electrolytes since the kinetics are also governed by the ion-conductivity, which generally follows the Butler-Volmer's equation assuming transference coefficients are 0.5.[34]

6.Ratio effect of electrolyte solvents, with same concentration of 1M $LiPF_6$

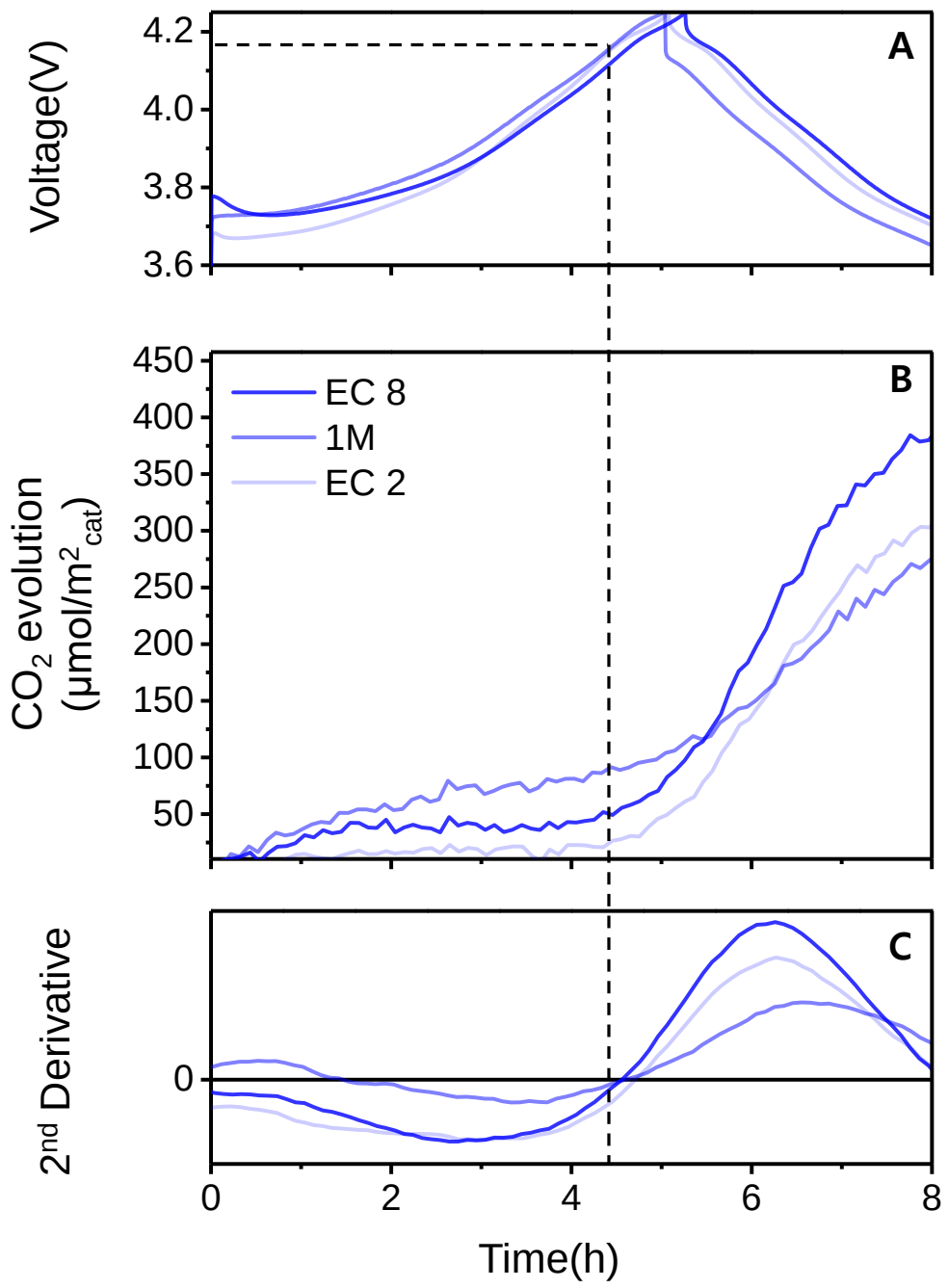

Supplementary Figure. 6: (A) Voltage profile of different electrolytes (B) in-situ CO_2 evolution representing lithium carbonate decomposition and (C) second derivative of CO_2 to verify start of evolution potential.

The effect of component ratio EC:DMC 2:8 (EC 2) ,5:5 (EC 5), and 8:2 (EC 8) in 1 M $LiPF_6$ is also investigated, although the exact mechanisms were not identified. The

amount of CO_2 gas is quantified with OEMS the start of evolution potential is slightly higher for EC 2, with start of evolution potential of 4.2 V, and EC 5 and EC 8 at 4.18 V vs Li/Li^{+}. The amount of gas evolved is comparable for all ratios of solvents, indicating similar decomposition reactions. This is both verified with OEMS and XPS data. Cyclability and EIS data also show that the three electrolytes with different ratios had similar decomposition of CO_2.

Surprisingly, there is little difference on the gas evolution, XPS, cyclability and EIS measurements, showing that it is likely that similar amounts of lithium carbonate had been decomposed. However, the coordination chemistry of electrolytes measured by Raman spectroscopy in Supplementary Figure. 7A is very different. The ratio of lithium solvated EC and free EC could be shown by comparing the relative intensities of 890 cm^{-1} and 918 cm^{-1}. Whereas there were very low intensities of lithium solvated EC compared to free EC in low concentrations, all three concentrations had relatively high intensities of lithium solvated intensities relative to free EC even at high solvent ratios

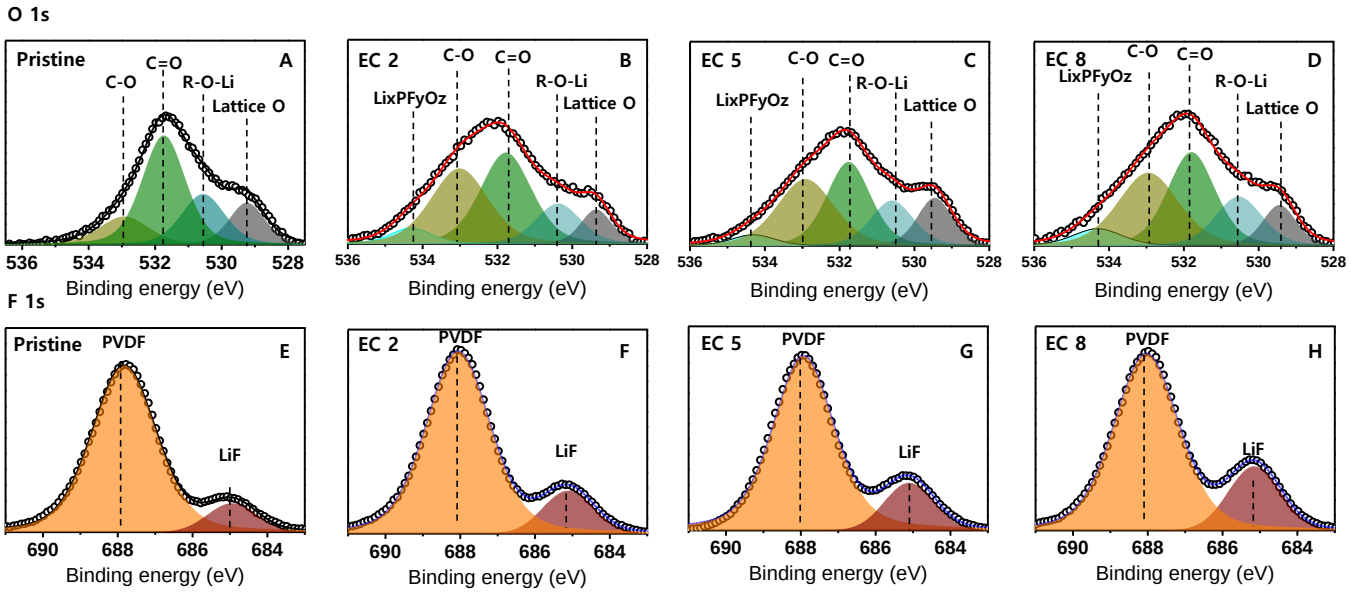

Supplementary Figure. 7: XPS O 1s spectra of (A) pristine, after 3 cycles of 0.2 C 3.0 V - 4.3 V samples of EC: DMC (B) 2:8 (C) 5:5 (D) 8:2. F 1S spectra of (E) pristine and after 3 cycles of 0.2 C 3.0 V - 4.3 V samples of EC: DMC (F) 2:8 (G) 5:5 and (H) 8:2

such as EC 8. This could support our hypothesis indirectly that the free EC states are responsible for the lowered kinetic barrier, since the large quantity of lithium solvated states would hinder activation of decomposition. However additional experiments on different ratios of low and high concentrations are needed to verify this phenomenon.

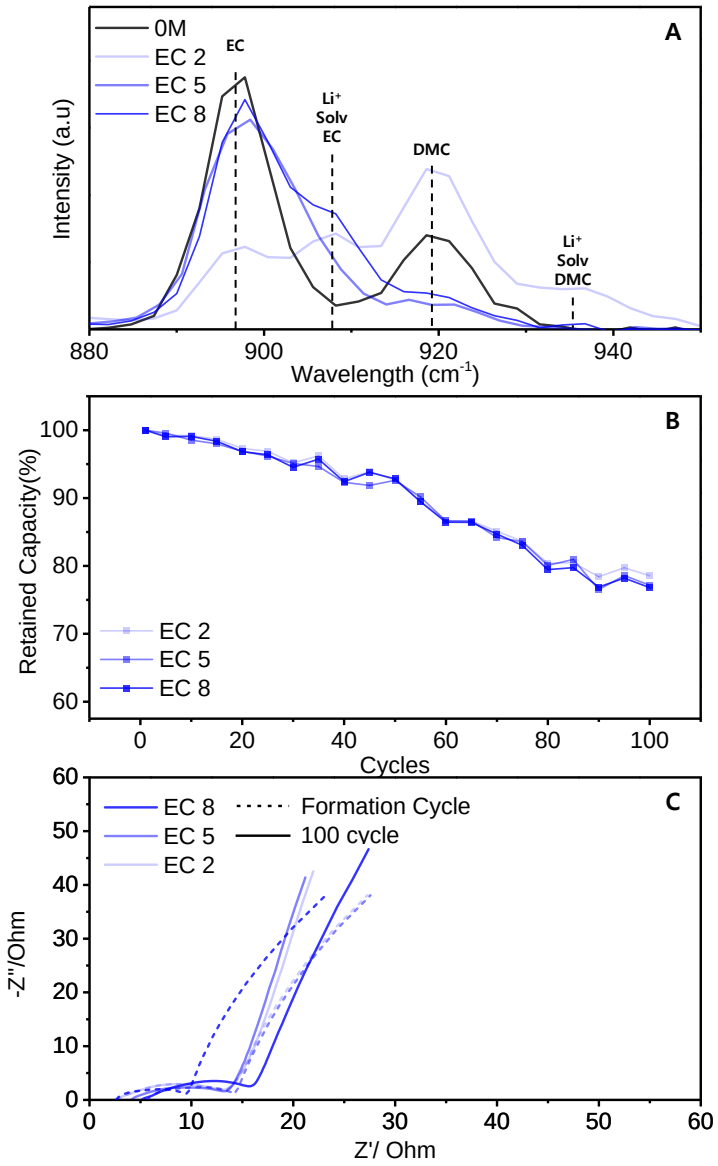

Supplementary Figure. 8: (A) Raman data of corresponding ratios (B) retained capacity and (C) relevant EIS data.

6.OEMS development appendix

The developing process of the online electrochemical mass spectrometry device is explained in this appendix. The goal of our development is to be able to qualitatively and quantitively measure side reactions of gas species of battery cells while operating the cell in realistic conditions. This is a challenging task since the application to battery cells required specific adjustments to the more commercially used Differential Electrochemical Mass Spectrometer (DEMS) utilized in many catalytic fields. Compared with the popular DEMS device, OEMS devices for battery gaseous measurements are not available commercially. Each OEMS is lab-made, and therefore every OEMS device has some advantages and some disadvantages over other researcher's setups. The focus of our system was to quantify small quantities of gas produced in realistic systems. Our system has advantages over other devices that the battery can be cycled realistically, and the electrochemical data is comparable to other commercial battery cell designs. It also has advantages in the detecting limit, being able to detect trace gases such as lattice oxygen evolution. The disadvantages of our system, however, is the limited range of experimental time. Our system with the current setup is only applicable within experiments that are ~20 hours. Therefore, the setup cannot be applied to a study of long-term cycles within LIBS.

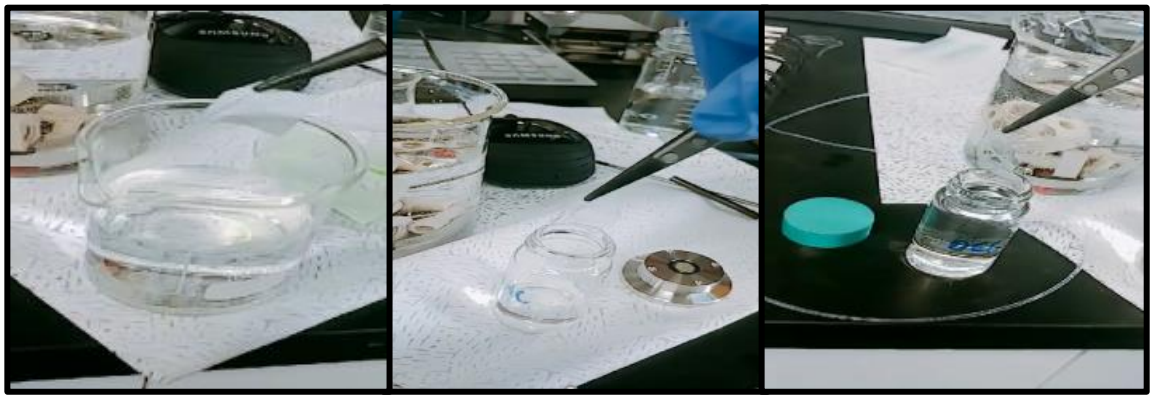

<H_2O>　　<DMC>　　<DEC>

Appendix Figure. 1:Wettability of PTFE with various solvents

The major difference of DEMS and OEMS is the sample introducing method. DEMS applies a Polytetrafluoroethylene (PTFE) membrane that separates the hydrophilic electrolyte from the high vacuum of the mass spectrometer. Gaseous species can pass through the pores of the PTFE membrane and be directly introduced to the mass spectrometer sample, hence giving the name “Differential”. This method has many advantages because of its low latency and high signal to noise ratio. However, the problem of this setup is that the crucial membrane implied in the experiment cannot be applicable to hydrophobic solvents. The hydrophobic PTFE is likely to become adsorbed by battery solvents such as DMC or DEC (diethyl carbonate). Therefore, rather than gaseous products introduced to the mass spectrometer, solvent species directly pass through the membrane causing serious damage to the vacuum system. The first attempt was to apply this DEMS system to gas analysis but was unsuccessful. Not only did the PTFE fail to prevent introduction of solvents, but the flow cell system implied with this system was also not gas-tight and continuously introduced large quantities of ambient air. This made it difficult to quantify the gases produced, as well as introducing unwanted reactions with the introduction of ambient air.

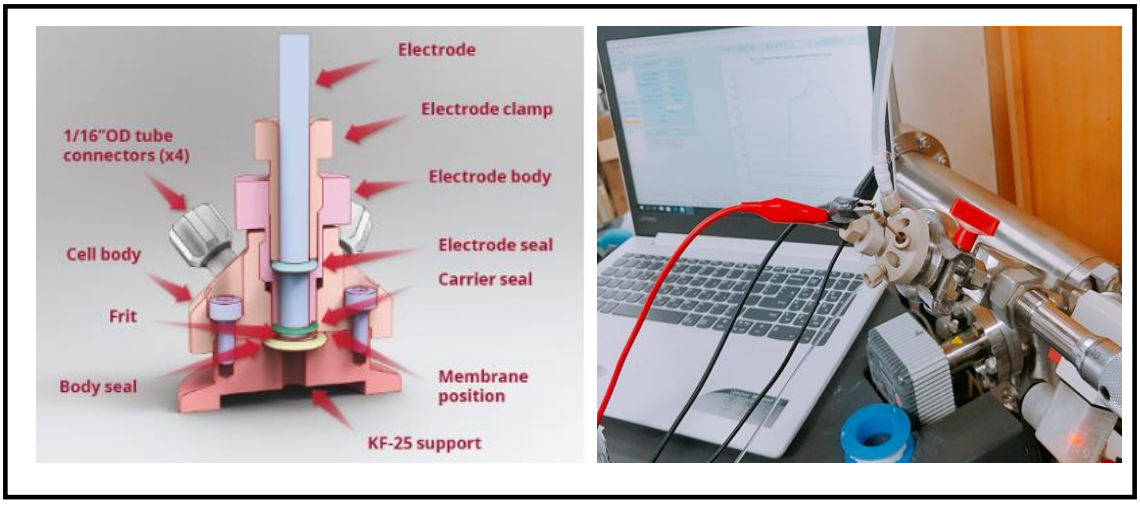

Appendix Figure. 2: First cell design: A electrolyte flowing system with PTFE membrane and the actual picture of the cell in operation. The flow cell design and membrane had major problems of air introduction and solvent introduction to the mass spectrometer.

To solve this problem, many researchers proposed other sampling methods. [40,41,16] The most appealing of all was the use of a standard leak that has a known flow rate of known gas in a known pressure difference[16]. This was the model system that we tried to build upon. The introduction of this standard leak had partial success, and we were able to detect most of the gaseous species reported to evolve in battery cells with this system.

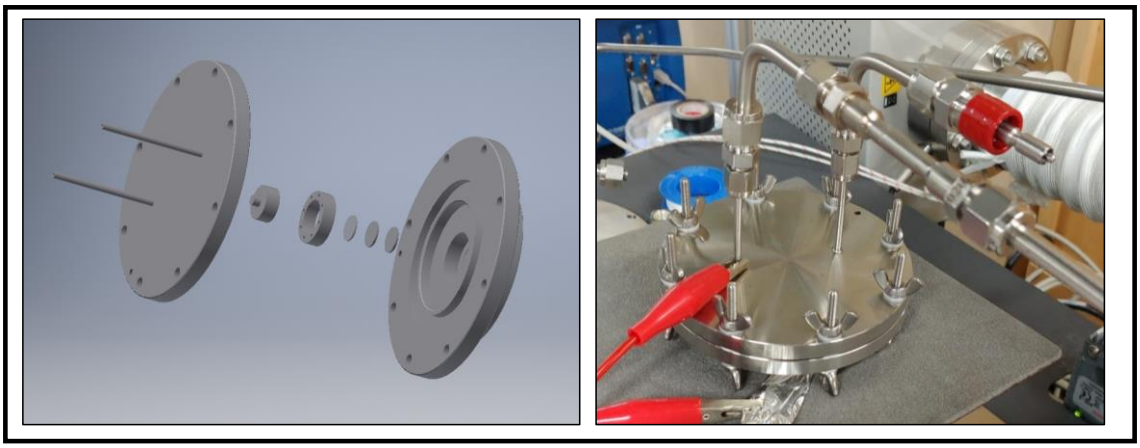

Appendix Figure. 3: Second cell design.

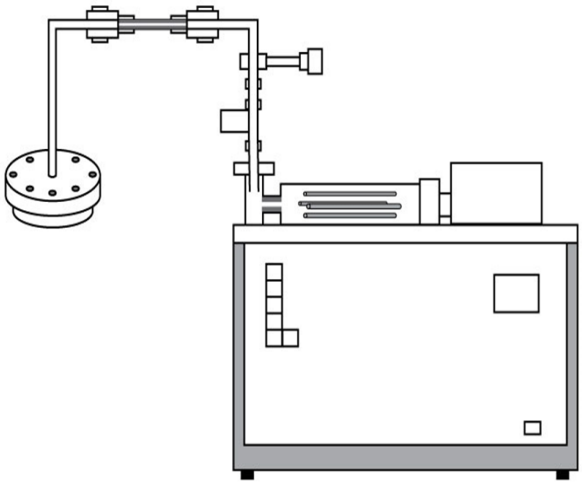

Appendix Figure. 4: Schematic sketch of our OEMS system

With the second cell design and interface, we were able to detect repetitive signals of gaseous products that evolved at high voltages. To match the electrochemical data and gaseous data, however, the latency between the voltage applied and the gas evolved must be synced. This was done with a RuO_2 oxygen evolution catalyst.

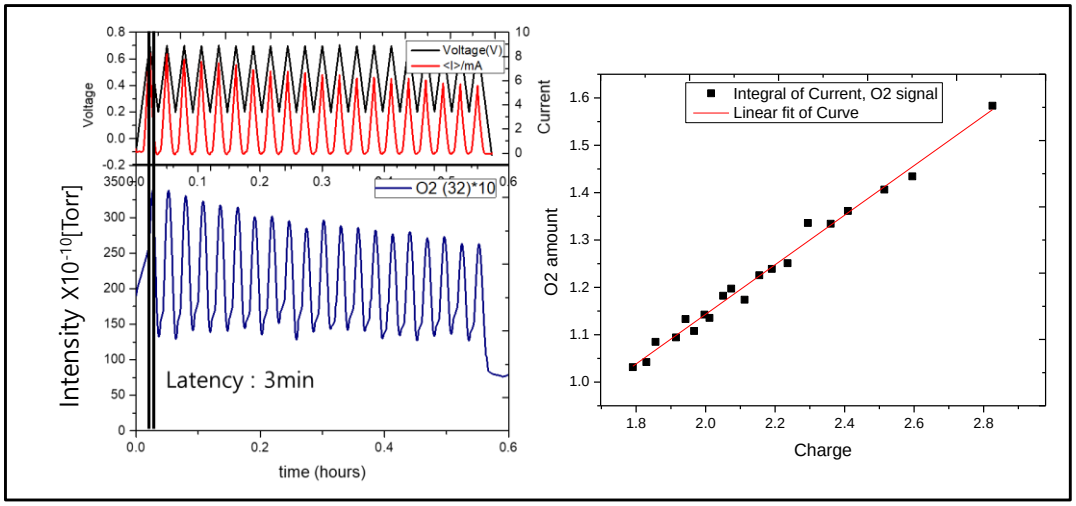

Appendix Figure. 5: OER using RuO2 catalyst. The total current and the integral of O2 signals were directly proportional.

By an extended CV cycle, the latency of our system was measured, and were 3 minutes

for the specific setup. The correspondence with current and oxygen intensities showed that our system gave proportional signals to the gases that have evolved. Using this data, other battery setups were experimented.

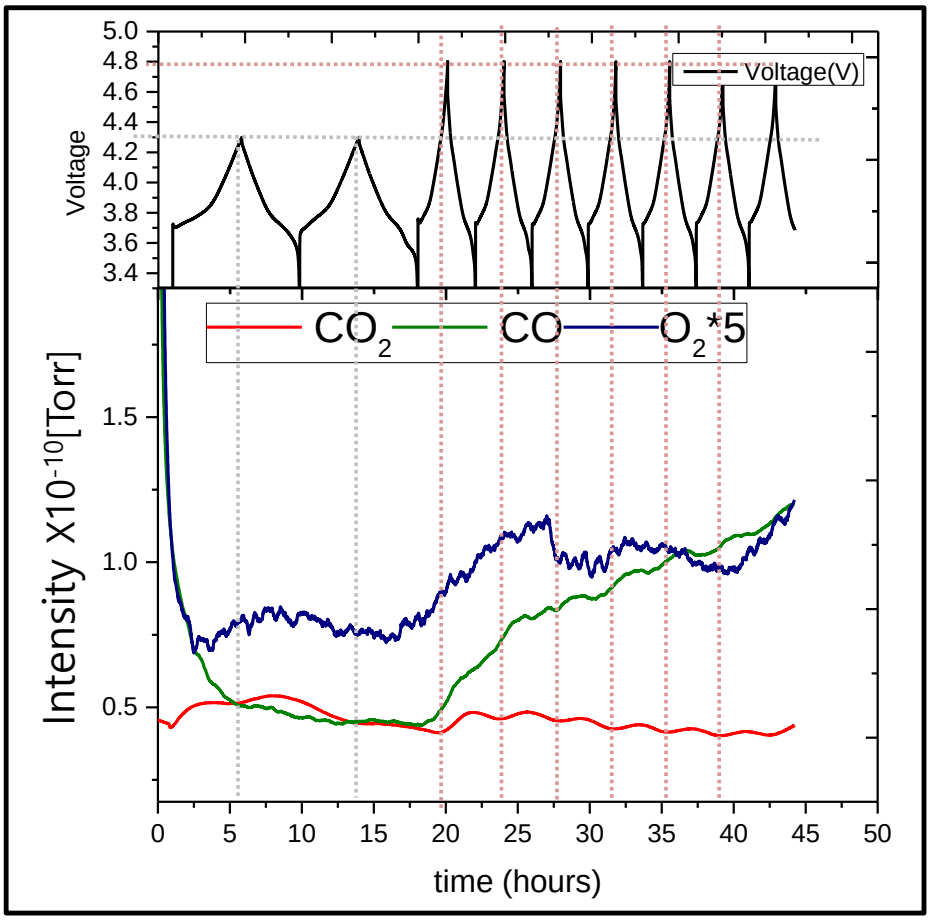

Appendix Figure. 6:second cell gas evolution of various gas species depending on voltage profile. There is no correlation of 4.8 V and oxygen evolution.

As seen in Appendix Figure. 6, major gaseous products including carbon dioxide and carbon monoxide were detected in correspondence with the voltage. However, the signal to noise ratio of the system was not sufficient to detect oxygen evolution yet. To solve this problem, three major changes were applied. The first is that a standard leak that had increased flowrate was used. The flowrate of the standard leak was increased from 0.1µl/s, to 1ul/s. Another difference was the increase in cell size, increasing the quantity of cathode used ~10 times. The last change is the decrease of head space from ~25cm^3 to

5.3cm^3 which had influences on the amount of sample introduced compared with the background Argon.

The combined effect had increased the signal to noise ratio of at least 2 orders.

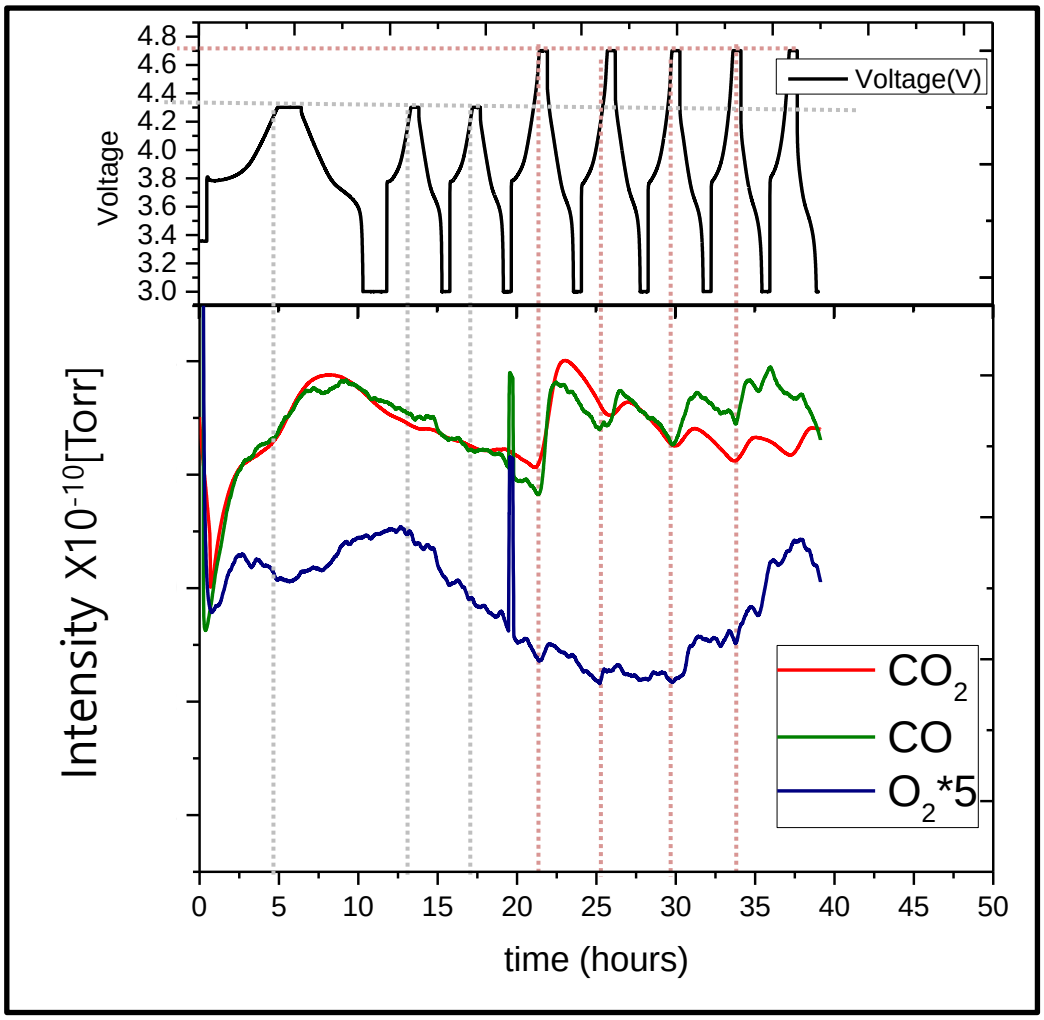

Appendix Figure. 7: third cell gas evolution of various gas species depending on voltage profile. Some correlation of 4.8 V and oxygen evolution is shown, although the fluctuating background makes it difficult to quantify the gas species evolved.

Appendix Figure. 7 show the typical raw data signals from the third and final design. Compared to the second cell design data, the intensity changes are much more dramatic. Also, the correlation of oxygen evolution is observed with high voltages, although the background signal modification is still required. This cell design is described in detail in

Supplementary data 1. Quantification methods are also explained in Supplementary data 4. All data are quantified by considering the total gas pressure and mass spectrometer signals and converting the signals within the dynamic range of the experiment.

7.Reference

1. Gröger, O., Gasteiger, H. A. & Suchsland, J.-P. Review—Electromobility: Batteries or Fuel Cells? *J. Electrochem. Soc.* **162**, A2605–A2622 (2015).

2. Blomgren, G. E. The Development and Future of Lithium Ion Batteries. *J. Electrochem. Soc.* **164**, A5019–A5025 (2017).

3. Myung, S. T. *et al.* Nickel-Rich Layered Cathode Materials for Automotive Lithium-Ion Batteries: Achievements and Perspectives. *ACS Energy Letters* vol. 2 196–223 (2017).

4. Freiberg, A. T. S., Sicklinger, J., Solchenbach, S. & Gasteiger, H. A. Li2CO3 decomposition in Li-ion batteries induced by the electrochemical oxidation of the electrolyte and of electrolyte impurities. *Electrochim. Acta* **346**, 136271 (2020).

5. Arai, H., Okada, S., Ohtsuka, H., Ichimura, M. & Yamaki, J. Characterization and cathode performance of Li1 - xNi1 + xO2 prepared with the excess lithium method. *Solid State Ionics* **80**, 261–269 (1995).

6. Sicklinger, J., Metzger, M., Beyer, H., Pritzl, D. & Gasteiger, H. A. Ambient Storage Derived Surface Contamination of NCM811 and NCM111: Performance Implications and Mitigation Strategies. *J. Electrochem. Soc.* **166**, A2322–A2335 (2019).

7. Shkrob, I. A. *et al.* Chemical Weathering of Layered Ni-Rich Oxide Electrode Materials: Evidence for Cation Exchange. *J. Electrochem. Soc.* **164**, A1489–A1498 (2017).

8. Cho, D.-H. *et al.* Effect of Residual Lithium Compounds on Layer Ni-Rich

Li[Ni 0.7 Mn 0.3]O 2 . *J. Electrochem. Soc.* **161**, A920–A926 (2014).

9. Noh, H. J., Youn, S., Yoon, C. S. & Sun, Y. K. Comparison of the structural and electrochemical properties of layered Li[NixCoyMnz]O2 (x = 1/3, 0.5, 0.6, 0.7, 0.8 and 0.85) cathode material for lithium-ion batteries. *J. Power Sources* **233**, 121–130 (2013).

10. Mahne, N., Renfrew, S. E., McCloskey, B. D. & Freunberger, S. A. Electrochemical Oxidation of Lithium Carbonate Generates Singlet Oxygen. *Angew. Chemie Int. Ed.* **57**, 5529–5533 (2018).

11. Bi, Y. *et al.* Stability of Li2CO3 in cathode of lithium ion battery and its influence on electrochemical performance. *RSC Adv.* **6**, 19233–19237 (2016).

12. Pritzl, D. *et al.* Editors' Choice—Washing of Nickel-Rich Cathode Materials for Lithium-Ion Batteries: Towards a Mechanistic Understanding. *J. Electrochem. Soc.* **166**, A4056–A4066 (2019).

13. Liu, Q. *et al.* Effects of a High-Concentration LiPF6-Based Carbonate Ester Electrolyte for the Electrochemical Performance of a High-Voltage Layered LiNi0.6Co0.2Mn0.2O2 Cathode. *ACS Appl. Energy Mater.* **2**, 8878–8884 (2019).

14. Girard, G. M. A. *et al.* Role of Li concentration and the SEI layer in enabling high performance Li metal electrodes using a phosphonium bis(fluorosulfonyl)imide ionic liquid. *J. Phys. Chem. C* **121**, 21087–21095 (2017).

15. Wang, M. *et al.* Effect of LiFSI Concentrations to Form Thickness- and Modulus-Controlled SEI Layers on Lithium Metal Anodes. *J. Phys. Chem. C*

122, 9825–9834 (2018).

16. Tsiouvaras, N., Meini, S., Buchberger, I. & Gasteiger, H. A. A Novel On-Line Mass Spectrometer Design for the Study of Multiple Charging Cycles of a Li-O 2 Battery . *J. Electrochem. Soc.* **160**, A471–A477 (2013).

17. Hatsukade, T., Schiele, A., Hartmann, P., Brezesinski, T. & Janek, J. Origin of Carbon Dioxide Evolved during Cycling of Nickel-Rich Layered NCM Cathodes. *ACS Appl. Mater. Interfaces* **10**, 38892–38899 (2018).

18. de Falco, G., Florent, M., De Rosa, A. & Bandosz, T. J. Proposing an unbiased oxygen reduction reaction onset potential determination by using a Savitzky-Golay differentiation procedure. *J. Colloid Interface Sci.* **586**, 597–600 (2020).

19. Meini, S. *et al.* Rechargeability of Li-air cathodes pre-filled with discharge products using an ether-based electrolyte solution: Implications for cycle-life of Li-air cells. *Phys. Chem. Chem. Phys.* **15**, 11478–11493 (2013).

20. Ling, C., Zhang, R., Takechi, K. & Mizuno, F. Intrinsic barrier to electrochemically decompose Li2CO3and LiOH. *J. Phys. Chem. C* **118**, 26591–26598 (2014).

21. Zhao, Z., Huang, J. & Peng, Z. Achilles' Heel of Lithium-Air Batteries: Lithium Carbonate. *Angew. Chemie Int. Ed.* **57**, 3874–3886 (2018).

22. Flores, E., Vonrüti, N., Novák, P., Aschauer, U. & Berg, E. J. Elucidation of LixNi0.8Co0.15Al0.05O2 Redox Chemistry by Operando Raman Spectroscopy. *Chem. Mater.* **30**, 4694–4703 (2018).

23. Li, Q. *et al.* Investigations on the Fundamental Process of Cathode Electrolyte

Interphase Formation and Evolution of High-Voltage Cathodes. *ACS Appl. Mater. Interfaces* **12**, 2319–2326 (2020).

24. Salitra, G. *et al.* High-Performance Cells Containing Lithium Metal Anodes, LiNi0.6Co0.2Mn0.2O2 (NCM 622) Cathodes, and Fluoroethylene Carbonate-Based Electrolyte Solution with Practical Loading. *ACS Appl. Mater. Interfaces* **10**, 19773–19782 (2018).

25. Liu, W. *et al.* Inhibition of transition metals dissolution in cobalt-free cathode with ultrathin robust interphase in concentrated electrolyte. *Nat. Commun.* **11**, (2020).

26. Jiao, S. *et al.* Stable cycling of high-voltage lithium metal batteries in ether electrolytes. *Nat. Energy* **3**, 739–746 (2018).

27. Xiong, X., Wang, Z., Yin, X., Guo, H. & Li, X. A modified LiF coating process to enhance the electrochemical performance characteristics of LiNi0.8Co0.1Mn0.1O 2 cathode materials. *Mater. Lett.* **110**, 4–9 (2013).

28. Guéguen, A. *et al.* Decomposition of LiPF 6 in High Energy Lithium-Ion Batteries Studied with Online Electrochemical Mass Spectrometry . *J. Electrochem. Soc.* **163**, A1095–A1100 (2016).

29. Morita, M., Asai, Y., Yoshimoto, N. & Ishikawa, M. *A Raman spectroscopic study of organic electrolyte solutions based on binary solvent systems of ethylene carbonate with low viscosity solvents which dissolve di ↑erent lithium salts*.

30. Lee, S.-I. *et al. A Study of Electrochemical Kinetics of Lithium Ion in Organic Electrolytes*. *Korean J. Chem. Eng* vol. 19 (2002).

31. Rodrigue Dougassa, Y., Jacquemin, J., El Ouatani, L. & Tessier, cile. Viscosity and Carbon Dioxide Solubility for LiPF 6 , LiTFSI, and LiFAP in Alkyl Carbonates: Lithium Salt Nature and Concentration Effect. (2014) doi:10.1021/jp500063c.

32. Wandt, J., Freiberg, A. T. S., Ogrodnik, A. & Gasteiger, H. A. Singlet oxygen evolution from layered transition metal oxide cathode materials and its implications for lithium-ion batteries. *Mater. Today* **21**, 825–833 (2018).

33. Ohashi, T., Okazaki, K. ichi, Fukunaga, T., Ogumi, Z. & Abe, T. Lithium-Ion Transfer at Cathode-Electrolyte Interface in Diluted Electrolytes Using Electrochemical Impedance Spectroscopy. *ChemElectroChem* **7**, 1644–1651 (2020).

34. Tatara, R. *et al.* The Effect of Electrode-Electrolyte Interface on the Electrochemical Impedance Spectra for Positive Electrode in Li-Ion Battery. *J. Electrochem. Soc.* **166**, A5090–A5098 (2019).

35. Mizusaki, J., Tagawa, H., Saito, K., Uchida, K. & Tezuka, M. Lithium carbonate as a solid electrolyte. *Solid State Ionics* **53**–**56**, 791–797 (1992).

36. Wang, H. *et al.* CO2 and O2 evolution at high voltage cathode materials of li-ion batteries: A differential electrochemical mass spectrometry study. *Anal. Chem.* **86**, 6197–6201 (2014).

37. Freiberg, A. T. S., Roos, M. K., Wandt, J., De Vivie-Riedle, R. & Gasteiger, H. A. Singlet Oxygen Reactivity with Carbonate Solvents Used for Li-Ion Battery Electrolytes. *J. Phys. Chem. A* **122**, 8828–8839 (2018).

38. Bouteau, G. *et al.* Effect of standard light illumination on electrolyte's stability of lithium-ion batteries based on ethylene and di-methyl carbonates. *Sci. Rep.* **9**, 1–9 (2019).

39. Bach, H. T., Meyer, B. A. & Tuggle, D. G. A Viscosity Equation for Gas Mixtures The. *Porous Media J. Chem. Phys.* **21**, 3199 (2003).

40. Berkes, B. B., Schiele, A., Sommer, H., Brezesinski, T. & Janek, J. On the gassing behavior of lithium-ion batteries with NCM523 cathodes. *J. Solid State Electrochem.* **20**, 2961–2967 (2016).

41. McCloskey, B. D., Bethune, D. S., Shelby, R. M., Girishkumar, G. & Luntz, A. C. Solvents critical role in nonaqueous Lithium-Oxygen battery electrochemistry. *J. Phys. Chem. Lett.* **2**, 1161–1166 (2011).

국문초록

전해질의 농도와 하이니켈 층상계 산화물에서의 잔여 리튬 카보네이트 안정성의 상관관계 분석

고동혁

분석화학

대학원

서울대학교

하이니켈 층상계 산화물은 리튬이온 배터리의 양극을 이루는 여러 후보 물질 중 우수한 에너지밀도를 가지고 있어 연구가 활발히 되고 있다. 그러나 이 물질은 그 합성과정에서 과량의 리튬 전구체를 사용하거나 보관중 공기접촉으로 인하여 표면에 리튬 카보네이트 잔여물이 많은 문제가 있다. 잔여 리튬 카보네이트가 분해되는 반응은 셀의 수명을 단축시키고, 가스 발생으로 인한 배터리의 안전문제와 직결되는 만큼 차세대 배터리의 개발에 있어서 중요한 문제 중 하나다. 잔여물을 없애기 위해 공정들이 추가되었지만, 잔여 리튬 카보네이트를 완벽히 없애는 것에는 많은 어려움이 따른다. 따라서 양극 표면에 존재하는 리튬 카보네이트의 분해반응을 억제하기 위하여, 이 반응을 이해하는 노력이 필요하다. 한편, 리튬 카보네이트

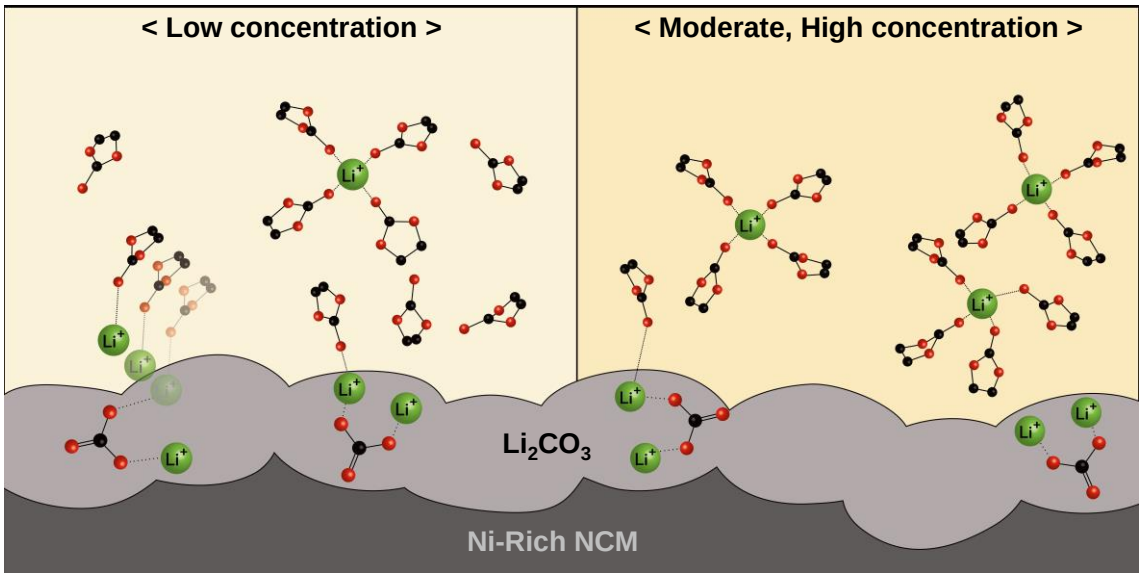

Scheme 1: Electrical decomposition of residual lithium carbonate facilitated by low concentration.

는 전해질과 접촉해 있으므로, 전해질의 성질이 잔여 리튬 카보네이트의 안정성에 영향을 주는 것은 자명하다. 그러나 이러한 중요성에도 불구하고 전해질이 잔여 리튬 카보네이트의 안정성에 미치는 영향은 아직까지 명확히 이해되지 않았다. 따라서, 이 연구는 전해질의 구성요소 중 염의 농도가 바뀜에 따라 안정성이 어떻게 달라지는 지 밝혀내는 데에 그 의의가 있다. Online electrochemical mass spectrometry (OEMS) 와 X-Ray Photoemission Spectroscopy (XPS)를 활용하여 우리는 배터리 구동에서 낮은 농도의 전해질이 리튬 카보네이트의 분해를 촉진시키는 것을 관찰하였다. 이러한 현상은 전해질 중 리튬이온을 용매화 하지 않은 자유 에틸렌 카보네이트가 리튬 카보네이트의 표면에 흡착하여 분해할 때의 활성화 에너지를 낮추는 효과 때문일 것으로 추정된다. 또한 낮은 농도의 배터리 구동에서 성능 저하가 고농도와 일반 농도에 비해 크다는 것을 보였고, 저농도에서는 이온 전달 임피던스가 배터리 구동 사이클에 따라 증가하는 것을 관찰하여 리튬 카보네이트의 분해반응이 배터리 구동에서 악영향을 끼치는 것을 확인하였다.